Dysfunctional brain reward system in child obesity

Jesus Pujol, MD[1,2*]; Laura Blanco-Hinojo, PhD[1,2]; Gerard Martínez-Vilavella, MSc[1]; Joan Deus, PhD[1,3]; Víctor Pérez-Sola, MD[2,4]; Jordi Sunyer, MD[5]

[1]MRI Research Unit, Department of Radiology, Hospital del Mar, Barcelona, Spain

[2]Centro Investigación Biomédica en Red de Salud Mental, CIBERSAM, Barcelona, Spain

[3]Department of Clinical and Health Psychology, Autonomous University of Barcelona, Spain.

[4]Institute of Neuropsychiatry and Addictions, Hospital del Mar- IMIM and Department of Psychiatry, Autonomous University of Barcelona, Barcelona, Spain.

[5]ISGlobal, Barcelona, Spain; Pompeu Fabra University, Barcelona, Catalonia, Spain; Ciber on Epidemiology and Public Health (CIBERESP), Madrid, Spain.

***Corresponding author:** Dr. Jesus Pujol. MRI Department, Hospital del Mar, Passeig Marítim 25-29. 08003, Barcelona, Spain. Email: 21404jpn@comb.cat Telephone: +34932212180 Fax: +34932212181

Abstract

Eating habits leading to obesity may reflect non-homeostatic behavior based on excessive immediate-reward seeking. However, it is currently unknown to what extent excess weight is associated with functional alterations in the brain's reward system in children. We tested the integrity of reward circuits using resting-state functional connectivity magnetic resonance imaging in a population of 230 children aged 8-12 years. The major components of the reward system were identified within the ventral striatum network defined on the basis of the nucleus accumbens connectivity pattern. The functional structure of the cerebral cortex was characterized using a combination of local functional connectivity measures. Higher body mass index was associated with weaker connectivity between the cortical and subcortical elements of the reward system, and enhanced integration of the sensorimotor cortex to superior parietal areas relevant to body image formation. Obese children, unlike WHO-defined overweight condition, showed functional structure alterations in the orbitofrontal cortex and amygdala region similar to those previously observed in primary obsessive-compulsive disorder and Prader Willi syndrome associated with obsessive eating behavior. Results further support the view that childhood obesity is not simply a deviant habit with restricted physical health consequences but is associated with reward system dysfunction characterizing behavioral control disorders.

Keywords: Eating behavior; obsessive-compulsive behavior; excess weight; ventral striatum; orbitofrontal cortex

Introduction

Childhood obesity is a major worldwide problem with harmful long-term health and occupational consequences, in addition to the adverse effect on the children's psychological wellbeing (NCD-RisC 2017; Lobstein, et al. 2004; WHO 2020). The epidemic spread of obesity is considered to be a consequence of non-healthy habits associated with a sedentary lifestyle and unbalanced diets (Lobstein et al. 2004; WHO 2020; Berthoud 2004). However, eating habits leading to obesity may ultimately reflect the non-homeostatic use of the reward system with an excess of immediate-reward seeking (Berthoud 2004; Moore et al. 2017; Volkow et al. 2013; Lennerz and Lennerz 2018; Stice et al. 2013; Kakoschke et al. 2019; Carter et al. 2016). In this study, we specifically investigated whether excess weight in children is associated with functional alterations in the brain's reward system.

Although the reward system has not yet been comprehensively assessed by means of resting-state functional connectivity measures in child populations, some data suggest that the system may be dysfunctional. Abnormal functional coupling has been reported between the middle frontal gyrus and ventral frontal cortices (Black et al. 2014). In adults or adolescents with excess weight, the evidence of functional connectivity alteration in the reward system is more compelling. Abnormal connectivity has been reported between the ventral striatum and functionally related frontal lobe areas (Contreras-Rodríguez et al. 2017a; Donofry et al. 2020; Coveleskie et al. 2015; Baek et al. 2017; Stoeckel et al. 2009), the orbitofrontal cortex and the middle temporal gyrus (Moreno-Lopez et al. 2016), core elements of the frontostriatal system and both the hypothalamus (Martín-Pérez et al. 2019; Contreras-Rodríguez et al. 2017b) and amygdala (Stoeckel et al. 2009; Dietrich et al. 2016), as well as between the amygdala/anterior hippocampus and the rest of the brain in terms of connectivity degree measures (Geha et al. 2017; Farruggia et al. 2020).

Such a variety of previous findings would indicate that the reward system is dysfunctional in the adult obese population. However, it is currently unknown to what extent excess weight is associated with functional alterations in the brain's reward system in developing children. Exploring the reward system may indeed be of particular interest in child populations during highly active shaping of neuronal connections prior to the formation of definitive personality traits (Cao et al. 2017; Khundrakpam et al. 2016; Larsen and Luna 2018).

We assessed a large sample of school children by combining both typical region-of-interest (seed) functional connectivity measures and a novel mapping of local cortical connections. Specifically, maps of the ventral striatum network were generated according to the resting-state connectivity pattern of the nucleus accumbens region, as a core subcortical element in the brain's reward system (Richard and Castro 2013; Wallis 2007). In addition, a multi-distance measure of local functional connectivity served to characterize the functional structure of the cerebral cortex (Macià et al. 2018). Using such imaging approaches, we previously identified functional alterations within the reward circuits in patients with obsessive-compulsive disorder (OCD) (Pujol et al. 2019) and in Prader-Willi syndrome, a genetic disorder that typically presents with both obsessive eating behavior and obesity (Pujol et al. 2016a). We primarily focused on determining whether body mass index (BMI) measures were incrementally associated with variations in functional connectivity (correlation analysis), and also tested for possible specific effects in terms of World Health Organization (WHO) weight categories (group analysis).

Methods

Participants

This present study forms part of a larger project designed to assess the effects of environmental factors on brain development (BREATHE, The European Commission: FP7-ERC-2010-AdG, ID 268479) (Pujol et al. 2016b). A total of 2,897 children participated in the whole survey based

on 39 schools, representative of the child population in the city of Barcelona. From this sample, 1,564 families were invited to participate in the MRI study via post, email or telephone, and 810 of them gave an initial positive response. Children were then consecutively recruited with the aim of including cases from all participating schools. Parents of 491 children were directly contacted. Consent to participate was finally not obtained in 165 cases, 27 children were lost before the assessment and 21 children were not eligible due to dental braces. A group of 278 children was therefore selected to participate in neuroimaging examinations, and a subgroup of 255 children completed anthropometric and imaging assessments.

A total of 230 cases were finally valid for the region-of-interest functional connectivity analysis (see below). The group included 115 boys and 115 girls and showed a mean age of 9.8 years (SD, 0.9 years; range, 8.0 to 12.1 years), and a mean BMI of 18.0 kg/m^2 (SD, 2.8 kg/m^2; range, 13.9 to 27.0 kg/m^2). A total of 147 (63.9%) children showed normal BMI, 50 (21.7%) belonged to the WHO overweight category and 33 (14.3%) to the WHO obese category (see below). No WHO-based underweight child was included in our study.

A total of 218 children were valid for the analysis of the cerebral cortex functional structure. This group included 105 boys and 113 girls and showed a mean age of 9.8 years (SD, 0.9 years; range 8.0 to 12.1 years), and a mean BMI of 18.0 kg/m2 (SD, 2.8 kg/m2; range, 13.9 to 27.0 kg/m2). A total of 139 (63.8%) children showed normal BMI, whilst 47 participants (21.6%) belonged to the WHO overweight category and 32 (14.7%) were obese.

All parents or tutors signed the informed consent form approved by the Research Ethical Committee (No. 2010/41221/I) of the IMIM-Parc de Salut Mar, Barcelona, Spain and the FP7-ERC-2010-AdG Ethics Review Committee (268479-22022011). The entire study was conducted in accordance with The Code of Ethics of the World Medical Association (Declaration of Helsinki).

Body mass index and WHO weight status

Child weight (kg) and height (m) were measured by trained researchers at school and served to calculate the BMI as weight/height^2 (Lobstein et al. 2004). BMI percentiles were then estimated adjusted to age and sex for each child by means of the WHO Growth Reference 2007 (de Onis et al. 2007; WHO 2007). The WHO categories were used to classify children according to adjusted BMI percentiles such as Normal or Healthy Weight (5th percentile to less than the 85th percentile), Overweight (85th percentile to less than the 95th percentile) and Obese (95th percentile or greater) (Barlow 2007). One Underweight (less than the 5th percentile) child was excluded from the study. Supplementary Figure 1 illustrates the distribution of BMI percentiles for participants included in both analyses.

MRI acquisition

We used a 1.5-T Signa Excite system (General Electric, Milwaukee, Wisconsin) equipped with an eight-channel phased-array head coil and single-shot echo-planar imaging (EPI) software. The functional sequence consisted of gradient recalled acquisition in the steady state (repetition time, 2000 ms; echo time, 50 ms; and pulse angle, 90º) in a 24-cm field of view, with a 64 x 64 pixel matrix and a slice thickness of 4 mm (interslice gap, 1.5 mm), voxel size 3.75 x 3.75 x 4 mm. Twenty-two interleaved sections, parallel to the anterior-posterior commissure line, were acquired to generate 180 whole-brain volumes, excluding 4 initial additional dummy volumes.

MRI exams were regularly acquired from 10 AM to 2 PM (exceptionally from 3 PM to 7 PM) at least 1 hour after the last meal. The resting-state functional MRI sequence lasted 6 minutes and was always the first sequence obtained, prior to the anatomical images. All participants were instructed to relax, stay awake, lie still and keep their eyes closed throughout the procedure. When contacted verbally immediately after the acquisition, we confirmed that there was no participant who had fallen asleep.

High-resolution 3D anatomical images were also obtained using an axial T1-weighted three-dimensional fast spoiled gradient inversion recovery-prepared sequence (repetition time 11.9 ms; echo time 4.2 ms; flip angle 15º; field of view 30 cm; 256 x 256 pixel matrix; slice thickness 1.2 mm; voxel size 1.17 x 1.17 x 1.2 mm), which served to assist functional connectivity image preprocessing. This sequence lasted 5 minutes and 40 seconds.

Anatomical and functional images were visually inspected to detect possible acquisition artifacts. Imaging data for both region-of-interest and IDAC analyses were subsequently processed using MATLAB version 2016a (The MathWorks Inc, Natick, Mass) and Statistical Parametric Mapping software (SPM12; The Wellcome Department of Imaging Neuroscience, London).

Region-of-interest (seed) functional connectivity mapping

Image preprocessing

This analysis was based on standard procedures previously adopted by our group (Harrison et al. 2009; Pujol et al. 2016b). Image preprocessing steps involved motion correction, spatial normalization and smoothing using a Gaussian filter (full-width half-maximum, 8 mm). Data were directly normalized to the standard SPM EPI template and re-sliced to 2 mm isotropic resolution in Montreal Neurological Institute (MNI) space. A Discrete Cosine Transform (DCT) filter was used to remove low frequency drifts below 0.008 Hz. In addition, we derived estimates of white matter, CSF and global brain signal fluctuations (using standard masks in MNI space from SPM) to include in the regression analyses as nuisance variables.

The procedures adopted to control for potential head motion effects included: (i) Conventional SPM time-series alignment to the first image volume in each subject. (ii) Exclusion of 24 children with outlier head motion, namely mean “inter-frame motion” greater than 0.12 mm. Mean inter-frame motion is a summary measure that combines mean translations and rotations across the scan (Pujol et al. 2014). (iii) The use of both motion-related regressors (i.e., 6 rigid

body realignment parameters) and estimates of global brain signal fluctuations (white matter, CSF and global brain signal) as confounding variables in first-level analyses. (iv) Within-subject, censoring-based MRI signal artifact removal (scrubbing) (Power et al. 2014) was used to discard motion-affected volumes. For each subject, mean inter-frame motion measures (Pujol et al., 2014) served as an index of data quality to flag volumes of suspect quality across the run. At time points with mean inter-frame motion > 0.2 mm, the corresponding volume, the immediately preceding and the succeeding two volumes were all discarded. Using this procedure, a mean of 12.2 (SD, 13.8; range, 0-61) volumes from the total of 180 volumes included in the functional MRI sequence were removed. (v) The use of the mean inter-frame motion across the fMRI run for each participant as a regressor in the second-level analyses (Pujol et al. 2014).

Estimation of seed maps

The identification of the reward system featured functional connectivity mapping of a basal ganglia region involving the nucleus accumbens. Based on a widely applied method for mapping basal ganglia functional connectivity, the region of interest (or 'seed') was centered at MNI coordinates (in mm) [x=±9, y=9, z=-8] (Harrison et al. 2009; Harrison et al. 2013). One single map of the reward system was obtained by averaging left and right ROI values.

The maps were generated by mean of previously described procedures (Harrison et al. 2013). Each seed region was defined as a 3.5 mm radial sphere (sampling ~ 25 voxels in 2 mm isotropic space) using the MarsBaR region of interest (ROI) toolbox in MNI stereotaxic space (Brett et al. 2003). Signals of interest were then extracted by calculating the mean ROI value at each time point across the series. To generate the seed maps, the signal time course of the selected seed region was used as a regressor to be correlated with the signal time course of each brain voxel with a view to generating first-level (single-subject) voxel-wise statistical parametric maps (contrast images).

Iso-Distant Average Correlation (IDAC) mapping

A novel mapping was used to characterize the functional structure of the cerebral cortex based on Iso-Distant Average Correlation (IDAC) measures. This imaging approach was proposed both to directly assess the cortical (frontal lobe) component of the reward system (Richard and Castro 2013; Wallis 2007) and to explore the entire cortex and tightly integrated structures such as the hippocampus and amygdala. Essentially, IDAC mapping expands well-established MRI measures of local functional connectivity (Sepulcre et al. 2010; Tomasi and Volkow 2010; Zang et al. 2004) by combining the connectivity maps of varying distances. Composite IDAC maps may uniquely inform the connectivity-related specialization of the cerebral cortex as local connectivity is distance-specific to a large extent and proved to discriminate well between major classical anatomo-functional cortical areas (Macia et al., 2018; Pujol et al., 2019).

Image preprocessing

Image preprocessing differed in some steps from that adopted in the conventional region-of-interest analysis to optimize the accuracy of short-distance functional connectivity measures. Functional MRI images were slice-time corrected, realigned and then smoothed using a narrow Gaussian filter (full-width half-maximum, 4 mm). Image volumes were then co-registered to their anatomical images with an affine transformation. A warping matrix was also estimated for every subject to match a group template created from the 3D anatomical individual acquisitions and then to the MNI space using DARTEL normalization (Ashburner, 2007). Image volumes were re-sliced to the relatively coarse 3x3x3 mm units to reduce the high computational loading. Estimated DARTEL normalizations to the MNI space were applied to the IDAC results to enable group inferences.

Analyses were conducted in a gray matter mask split into left and right hemispheres, so that no adjacent voxels from the medial regions of one hemisphere would be locally associated with

those from the other hemisphere. The two hemispheres were brought back together once the IDAC values had been calculated. The left and right hemisphere gray matter masks were obtained by setting a threshold of p>0.4 on the gray matter probability maps obtained from the DARTEL group template. As IDAC value estimations were carried out in every subject's native space, the template masks were back-transformed with the inverse estimated normalization.

As in the region-of-interest analysis, all time series were regressed on the 6 rigid body realignment parameters, and on the average white matter, CSF and global brain signals extracted from the native tissue masks. Finally, all functional MRI time series were band-passed with a DCT filter letting through frequencies in the 0.01-0.1 Hz interval.

The control for potential head motion effects was identical to that of the region-of-interest analysis (see above). After scrubbing, a mean of 12.1 (SD, 15.1; range, 0-61) volumes were removed. A total of 36 participants were excluded on the basis of imaging quality (mean inter-frame motion greater than 0.12 mm [n= 24] or sub-optimal 3D anatomical image quality in the form of signal loss or signal blurring related to motion [n= 12]).

Estimation of IDAC maps

Whole-cortex IDAC maps were generated by estimating the average temporal correlation of each voxel with all its neighboring voxels placed at increasingly separated Euclidean iso-distant intervals. IDAC was computed in native space separately for each hemisphere after realignment and smoothing. Three IDAC maps were obtained at distance intervals 5-10mm, 15-20mm and 25-30mm. The definition and mathematical formulation of IDAC measures are extensively described in our early report (Macia et al., 2018) and in the Supplementary Material.

Multi-distance IDAC color maps were generated from the overlay of the three IDAC maps using an RGB color codification (Suppl. Figure 2). RGB color channels permitted the display of

three values simultaneously. RED to display results from 5-10mm IDAC maps, GREEN from 15-20mm and BLUE from 25-30mm. The overlapping of these primary colors produces a full range of secondary colors, which provide information as to functional structure variations across cortical areas.

To establish a color-coding, each gray image corresponding to the three individual IDAC maps (5-10mm, 15-20mm and 25-30mm) was separately scaled to its maximal t value using conventional, automated SPM tools (Suppl. Figure 2). Composite RGB maps were generated from individual (three distances) one-sample IDAC maps, individual correlation maps and individual between-group comparison t-maps.

Statistical analysis

Correlation analysis. After individual preprocessing of each functional image sequence, separate second-level analyses were performed using SPM to map voxel-wise the across-subject correlation between BMI percentile and both reward system functional connectivity maps and IDAC maps (separately for each distance). A motion summary measure (inter-frame motion [Pujol et al. 2014]) for each participant was included as a nuisance variable.

Group analysis according to WHO weight categories. Voxel-wise group differences in functional connectivity for both ROI and IDAC approaches were evaluated in SPM using the Student's t-test within a random-effects ANOVA that also included the motion summary measure as a covariate of no interest. Analyses of interest included comparing the three groups, as well as the normal weight group with overweight and obese groups combined. WHO group [normal, overweight, obese] by distance [5-10mm, 15-20mm and 25-30mm] interactions were tested using a 3 x 3 full factorial ANOVA model.

In all analyses, results were considered significant when clusters formed at a threshold of $p < 0.005$ survived whole-brain family-wise error (FWE) correction ($p < 0.05$), calculated by means of SPM.

Results

Reward system network

In the correlation analysis, higher BMI percentiles were associated with *weaker* functional connectivity between the nucleus accumbens and both the orbitofrontal cortex and the sensorimotor cortex in the cortical representation of the body (Figure 1, Suppl. Table 1). The orbitofrontal cortex showing the significant effect is a core element of the reward system network (Suppl. Figure 3). In contrast, the implicated sensorimotor cortex is a region adjacent to superior parietal areas anticorrelated with the nucleus accumbens in normal-weight children, and is part of the nucleus accumbens anticorrelated map in children with excess weight (Figure 2).

The analysis comparing WHO weight categories showed that connectivity alterations between the nucleus accumbens and both orbitofrontal and sensorimotor areas were more evident in obese children. However, the changes were already present in overweight children, and the differences between overweight and obese groups were marginal and limited to a part of the sensorimotor cortex (Figure 3 and Suppl. Table 2).

Cerebral cortex functional structure

In the correlation analysis, higher BMI percentiles were associated with *stronger* local functional connectivity in a region involving the somatosensory cortex at the cortical representation of the body and the superior parietal cortex (Figure 4, Suppl. Table 3).

The group analysis showed that the alteration in the sensory cortices was already present in the overweight-child group or when combining overweight and obese groups, which showed significantly higher local functional connectivity than normal-weight children (Suppl. Table 4, Suppl. Figure 4). However, the effect was not specifically demonstrated for the obese category alone in the context of such findings.

Instead, obese children showed *weaker* local functional connectivity specifically in the orbitofrontal cortex and a circumscribed region implicating the anterior hippocampus, parahippocampal gyrus and amygdala (Figure 5 and Suppl. Table 5). The differences were notable between obese and overweight children in the orbitofrontal cortex, which would indicate that the WHO obese category is a qualitatively distinct condition in terms of orbitofrontal cortex functional alteration.

Specific assessment of the interaction between WHO weight categories and functional connectivity distances showed significant overall results (Suppl. Table 6). Post-hoc testing indicated that the functional connectivity of the orbitofrontal cortex and amygdala region was significantly weaker in obese children at local short distance (5-10mm) than local long distance (25-30mm) (Suppl. Figure 5, Suppl. Table 6). The analysis was, therefore, indicative of changes particularly in the functional structure of the regions, rather than expressing a general tendency of functional connectivity reduction.

Discussion

We investigated whether excess weight is associated with alteration in the functional integrity of the reward system in a large group of school children. We observed that higher BMI was associated with weaker functional connectivity between the ventral striatum and the orbitofrontal cortex, which are the core elements of the reward system. Higher BMI was also associated with increased integration of the sensorimotor cortex to superior parietal areas

relevant to bodily self-consciousness. Finally, obese children, unlike the overweight group, showed alterations in the functional structure of the orbitofrontal cortex and amygdala region. The results would, therefore, indicate that the reward system is dysfunctional in children with excess weight.

Each of the identified findings may express a distinct functional disturbance. Weaker functional coupling within the reward system has previously been reported in adult populations with excess weight (Donofry et al. 2020; Baek et al. 2017; Geha et al. 2017; Contreras-Rodríguez et al. 2017a). Weaker connectivity may express reduced tonic activity and may be the chronic consequence of reward system overstimulation (Volkow et al. 2013, Lennerz et al. 2018; Stice et al. 2018). However, weaker connectivity in the reward system at rest may combine with stronger connectivity during exposure to food-related cues (Donofry et al. 2020; Geha et al. 2017). Hyper-responses may be particularly evident in the dorsal aspects of the reward system and more related to food seeking and craving than to the reward itself (Volkow et al. 2013; Lennerz et al. 2018; Donofry et al. 2020). We observed that functional connectivity weakening between the elements of the reward system was already present in overweight (BMI percentile ≥ 85^{th}) children, which may suggest that the functional measure is both highly sensitive and most probably identifies the initial stage of reward system dysfunction.

We observed that higher BMI was linearly associated with weaker functional connectivity between the ventral striatum and the sensorimotor cortex, and that this cortical region showed a tendency to be integrated to the superior parietal cortex in children with excess weight. In addition, excess weight was associated with heightened local functional connectivity in similar areas in IDAC-measure analyses. Both types of findings may indicate that the somatosensory and motor cortical representation of the body is expanded as a function of body mass. Importantly, research in human cognitive neuroscience has indicated that the superior parietal cortex gathers a set of brain areas strongly linked to body image formation or bodily self-consciousness, which is the most somatic facet of self-consciousness (Blanke et al. 2015;

Ronchi et al. 2018). Our results may well suggest how self-perception could incrementally be distorted in children with excess weight, which could indeed contribute to altering the child's psychological wellbeing and ultimately increase the risk of developing body image disorders.

A qualitatively different functional connectivity alteration was identified in obese children, that was not present in the overweight group. Children with BMI percentile 95^{th} or greater showed reduced local functional connectivity within the orbitofrontal cortex and in a region involving the anterior hippocampus, parahippocampal gyrus and part of the amygdala, which are all major afferents of the nucleus accumbens/orbitofrontal cortex complex (Rolls,2019; Kim et al. 2017). We have recently reported a similar functional alteration in the orbitofrontal cortex in patients with typical OCD (Pujol et al. 2019). In the context of OCD, the dysfunctional trait was interpreted as expressing deficient cortical inhibition and was associated with the severity of obsessions and compulsions. Significantly, therefore, the observed alteration in the orbitofrontal cortex functional integrity in obese, albeit otherwise typically developing, children may be of a pathological nature overlapping with a major disorder characterized by compulsive behavior.

The results reported in the current study are also consistent with changes observed in the Prader Willi syndrome, which is a genetic disorder typically showing both obesity and obsessive-compulsive symptoms including severe compulsive eating. Altered functional coupling in the reward system was identified at rest (Zhang et al. 2013; Zhang et al. 2015; Lukoshe et al. 2017). We specifically reported a significant correlation between obsessive eating behavior and abnormal functional connectivity both within the basal ganglia circuits and between the ventral striatum and amygdala (Pujol et al. 2016a). Therefore, it may be of interest in future studies the use of behavioral testing to investigate whether child obesity is similarly associated with compulsive eating.

A limitation to our study relates to the use of a 1.5-T system, as opposed to a 3-T system with a higher MRI signal. Although we did have the 3-Tesla option, the present study was developed

using a 1.5-Tesla magnet following the recommendations of the FP7-ERC Ethics Review Committee to limit magnetic field strength in children. Our study was also limited in that impulse control performance and eating habits were not documented in our child sample. A comprehensive behavior assessment could have better characterized the dysfunctional process in the reward system.

The set of alterations identified in our child cohort may therefore indicate that the reward system does not work properly in children with excess weight showing some pathophysiological features compatible with typical obsessive-compulsive disorders, particularly in the WHO-defined obese condition. Our study cannot solve the extent to which the functional disturbance is a primary event that predisposes individuals to obesity, or a consequence of the deviant habits or, indeed, a combination of both factors. However, the dysfunctional status may ultimately interfere with the normal development of the reward system and favor more permanent brain damage. We would, therefore, further emphasize the need for early intervention in child obesity before body image and personality traits are fully established.

Funding: This work was supported in part by the European Research Council under the ERC [grant number 268479] – the BREATHE project.

Acknowledgments: We thank the Agency of University and Research Funding Management of the Catalonia Government for their participation in the context of Research Groups SGR2017_134 and SGR2017_1198.

Conflicts of interest: Drs. Jesus Pujol, Laura Blanco-Hinojo, Gerard Martínez-Vilavella, Joan Deus, Víctor Pérez-Sola and Jordi Sunyer report no competing interests.

References

Ashburner J. (2007). A fast diffeomorphic image registration algorithm. *NeuroImage*, 38(1), 95–113.

Baek, K., Morris, L. S., Kundu, P., & Voon, V. (2017). Disrupted resting-state brain network properties in obesity: decreased global and putaminal cortico-striatal network efficiency. *Psychological Medicine*, 47(4), 585–596.

Barlow, S.E. (2007). Expert Committee. Expert committee recommendations regarding the prevention, assessment, and treatment of child and adolescent overweight and obesity: summary report. *Pediatrics*, 120 Suppl 4:S164-92.

Berthoud, H. R. (2004). Neural control of appetite: cross-talk between homeostatic and non-homeostatic systems. *Appetite*, 43(3), 315–317.

Black, W. R., Lepping, R. J., Bruce, A. S., Powell, J. N., Bruce, J. M., Martin, L. E., Davis, A. M., Brooks, W. M., Savage, C. R., & Simmons, W. K. (2014). Tonic hyper-connectivity of reward neurocircuitry in obese children. *Obesity*, 22(7), 1590–1593.

Blanke, O., Slater, M., & Serino, A. (2015). Behavioral, Neural, and Computational Principles of Bodily Self-Consciousness. *Neuron*, 88(1), 145–166.

Brett, M., Valabregue, R. & Poline, J. (2003). Region of Interest analysis using an SPM toolbox. *NeuroImage*, 16(Suppl.).

Cao, M., Huang, H. & He, Y. (2017). Developmental connectomics from infancy through early childhood. *Trends in Neuroscience*, 40(8), 494–506.

Carter, A., Hendrikse, J., Lee, N., Yücel, M., Verdejo-Garcia, A., Andrews, Z. B., & Hall, W. (2016). The Neurobiology of "Food Addiction" and Its Implications for Obesity Treatment and Policy. *Annual Review of Nutrition*, 36, 105–128.

Contreras-Rodríguez, O., Martín-Pérez, C., Vilar-López, R., & Verdejo-Garcia, A. (2017a). Ventral and Dorsal Striatum Networks in Obesity: Link to Food Craving and Weight Gain. *Biological Psychiatry*, 81(9), 789–796.

Contreras-Rodríguez, O., Vilar-López, R., Andrews, Z. B., Navas, J. F., Soriano-Mas, C., & Verdejo-García, A. (2017b). Altered cross-talk between the hypothalamus and non-homeostatic regions linked to obesity and difficulty to lose weight. *Scientific Reports*, 7(1), 9951.

Coveleskie, K., Gupta, A., Kilpatrick, L. A., Mayer, E. D., Ashe-McNalley, C., Stains, J., Labus, J. S., & Mayer, E. A. (2015). Altered functional connectivity within the central reward network in overweight and obese women. *Nutrition & Dabetes*, 5(1), e148.

de Onis, M., Onyango, A. W., Borghi, E., Siyam, A., Nishida, C., & Siekmann, J. (2007). Development of a WHO growth reference for school-aged children and adolescents. *Bulletin of the World Health Organization*, 85(9), 660–667.

Dietrich, A., Hollmann, M., Mathar, D., Villringer, A., & Horstmann, A. (2016). Brain regulation of food craving: relationships with weight status and eating behavior. *International Journal of Obesity* (2005), 40(6), 982–989.

Donofry, S. D., Jakicic, J. M., Rogers, R. J., Watt, J. C., Roecklein, K. A., & Erickson, K. I. (2020). Comparison of Food Cue-Evoked and Resting-State Functional Connectivity in Obesity. *Psychosomatic Medicine*, 82(3), 261–271.

Farruggia, M. C., van Kooten, M. J., Perszyk, E. E., Burke, M. V., Scheinost, D., Constable, R. T., & Small, D. M. (2020). Identification of a brain fingerprint for overweight and obesity. *Physiology & Behavior*, 222, 112940.

Geha, P., Cecchi, G., Todd Constable, R., Abdallah, C., & Small, D. M. (2017). Reorganization of brain connectivity in obesity. *Human Brain Mapping*, 38(3), 1403–1420.

Harrison, B. J., Pujol, J., Cardoner, N., Deus, J., Alonso, P., López-Solà, M., Contreras-Rodríguez, O., Real, E., Segalàs, C., Blanco-Hinojo, L., Menchon, J. M., & Soriano-Mas, C. (2013). Brain corticostriatal systems and the major clinical symptom dimensions of obsessive-compulsive disorder. *Biological Psychiatry*, 73(4), 321–328.

Harrison, B. J., Soriano-Mas, C., Pujol, J., Ortiz, H., López-Solà, M., Hernández-Ribas, R., Deus, J., Alonso, P., Yücel, M., Pantelis, C., Menchon, J. M., & Cardoner, N. (2009). Altered corticostriatal functional connectivity in obsessive-compulsive disorder. *Archives of General Psychiatry*, 66(11), 1189–1200.

Kakoschke, N., Aarts, E., & Verdejo-García, A. (2019). The Cognitive Drivers of Compulsive Eating Behavior. *Frontiers in Behavioral Neuroscience*, 12, 338.

Khundrakpam, B.S., Lewis, J.D., Zhao, L., Chouinard-Decorte, F. & Evans, A.C. (2016). Brain connectivity in normally developing children and adolescents. *Neuroimage,* 34, 192–203.

Kim, H. J., Lee, J. H., Yun, K., & Kim, J. H. (2017). Alterations in Striatal Circuits Underlying Addiction-Like Behaviors. *Molecules and Cells*, 40(6), 379–385.

Larsen, B. & Luna, B. (2018). Adolescence as a neurobiological critical period for the development of higher-order cognition. *Neuroscience & Biobehavioral Reviews*, 94, 179–195.

Lennerz, B., & Lennerz, J. K. (2018). Food Addiction, High-Glycemic-Index Carbohydrates, and Obesity. *Clinical chemistry*, 64(1), 64–71.

Lobstein, T., Baur, L., Uauy, R., & IASO International Obesity TaskForce. (2004). Obesity in children and young people: A crisis in public health. *Obesity reviews*, 5 Suppl 1, 4-104.

Lukoshe, A., van Dijk, S. E., van den Bosch, G. E., van der Lugt, A., White, T., & Hokken-Koelega, A. C. (2017). Altered functional resting-state hypothalamic connectivity and abnormal pituitary morphology in children with Prader-Willi syndrome. *Journal of Neurodevelopmental Disorders*, 9, 12.

Macià, D., Pujol, J., Blanco-Hinojo, L., Martínez-Vilavella, G., Martín-Santos, R., & Deus, J. (2018). Characterization of the Spatial Structure of Local Functional Connectivity Using Multidistance Average Correlation Measures. *Brain Connectivity*, 8(5), 276–287.

Martín-Pérez, C., Contreras-Rodríguez, O., Vilar-López, R., & Verdejo-García, A. (2019). Hypothalamic Networks in Adolescents With Excess Weight: Stress-Related Connectivity and Associations With Emotional Eating. *Journal of the American Academy of Child and Adolescent Psychiatry*, 58(2), 211–220.e5.

Moore, C. F., Sabino, V., Koob, G. F., & Cottone, P. (2017). Pathological Overeating: Emerging Evidence for a Compulsivity Construct. *Neuropsychopharmacology*; 42(7), 1375–1389.

Moreno-Lopez, L., Contreras-Rodriguez, O., Soriano-Mas, C., Stamatakis, E. A., & Verdejo-Garcia, A. (2016). Disrupted functional connectivity in adolescent obesity. *NeuroImage. Clinical*, 12, 262–268.

NCD Risk Factor Collaboration (NCD-RisC). (2017). Worldwide Trends in Body-Mass Index, Underweight, Overweight, and Obesity From 1975 to 2016: A Pooled Analysis of 2416 Population-Based Measurement Studies in 128.9 Million Children, Adolescents, and Adults. *Lancet*, 390, 2627-2642.

Power, J. D., Mitra, A., Laumann, T. O., Snyder, A. Z., Schlaggar, B. L., & Petersen, S. E. (2014). Methods to detect, characterize, and remove motion artifact in resting state fMRI. *NeuroImage*, 84, 320–341.

Pujol, J., Blanco-Hinojo, L., Esteba-Castillo, S., Caixàs, A., Harrison, B. J., Bueno, M., Deus, J., Rigla, M., Macià, D., Llorente-Onaindia, J., & Novell-Alsina, R. (2016a). Anomalous basal ganglia connectivity and obsessive-compulsive behaviour in patients with Prader Willi syndrome. *Journal of Psychiatry & Neuroscience*, 41(4), 261–271.

Pujol, J., Blanco-Hinojo, L., Maciá, D., Alonso, P., Harrison, B. J., Martínez-Vilavella, G., Deus, J., Menchón, J. M., Cardoner, N., & Soriano-Mas, C. (2019). Mapping Alterations of the Functional Structure of the Cerebral Cortex in Obsessive-Compulsive Disorder. *Cerebral Cortex*, 29(11), 4753–4762.

Pujol, J., Macià, D., Blanco-Hinojo, L., Martínez-Vilavella, G., Sunyer, J., de la Torre, R., Caixàs, A., Martín-Santos, R., Deus, J., & Harrison, B. J. (2014). Does motion-related brain functional connectivity reflect both artifacts and genuine neural activity?. *NeuroImage*, 101, 87–95.

Pujol, J., Martínez-Vilavella, G., Macià, D., Fenoll, R., Alvarez-Pedrerol, M., Rivas, I., Forns, J., Blanco-Hinojo, L., Capellades, J., Querol, X., Deus, J., & Sunyer, J. (2016b). Traffic pollution exposure is associated with altered brain connectivity in school children. *NeuroImage*, 129, 175–184.

Richard, J. M., Castro, D. C., Difeliceantonio, A. G., Robinson, M. J., & Berridge, K. C. (2013). Mapping brain circuits of reward and motivation: in the footsteps of Ann Kelley. *Neuroscience and Biobehavioral Reviews*, 37(9 Pt A), 1919–1931.

Rolls E. T. (2019). The orbitofrontal cortex and emotion in health and disease, including depression. *Neuropsychologia*, 128, 14–43.

Ronchi, R., Park, H. D., & Blanke, O. (2018). Bodily self-consciousness and its disorders. *Handbook of Clinical Neurology*, 151, 313–330.

Sepulcre, J., Liu, H., Talukdar, T., Martincorena, I., Yeo, B.T. & Buckner R.L. (2010). The organization of local and distant functional connectivity in the human brain. *PLoS Computational Biology*, 6(6), e1000808.

Stice, E., Figlewicz, D. P., Gosnell, B. A., Levine, A. S., & Pratt, W. E. (2013). The contribution of brain reward circuits to the obesity epidemic. *Neuroscience and Biobehavioral Reviews*, 37(9 Pt A), 2047–2058.

Stoeckel, L. E., Kim, J., Weller, R. E., Cox, J. E., Cook, E. W., 3rd, & Horwitz, B. (2009). Effective connectivity of a reward network in obese women. *Brain Research Bulletin*, 79(6), 388–395.

Tomasi, D. & Volkow, N.D. (2010). Functional connectivity density mapping. *Proceedings of the National Academy of Sciences of the USA*, 107(21), 9885–9890.

Volkow, N. D., Wang, G. J., Tomasi, D., & Baler, R. D. (2013). The addictive dimensionality of obesity. *Biological psychiatry*, 73(9), 811–818.

Wallis J. D. (2007). Orbitofrontal cortex and its contribution to decision-making. *Annual Review of Neuroscience*, 30, 31–56.

WHO Growth reference 5-19 years. BMI-for-age (5-19 years). https://www.who.int/growthref/who2007_bmi_for_age/en/. Accessed June 10, 2020.

World Health Organization. Obesity and overweight. 1 April 2020. Available at: https://www.who.int/news-room/fact-sheets/detail/obesity-and-overweight. Accessed June 10, 2020.

Zang, Y., Jiang, T., Lu, Y., He, Y. & Tian, L. (2004). Regional homogeneity approach to fMRI data analysis. *Neuroimage*, 22(1), 394–400.

Zhang, Y., Wang, J., Zhang, G., Zhu, Q., Cai, W., Tian, J., Zhang, Y. E., Miller, J. L., Wen, X., Ding, M., Gold, M. S., & Liu, Y. (2015). The neurobiological drive for overeating implicated in Prader-Willi syndrome. *Brain Research*, 1620, 72–80.

Zhang, Y., Zhao, H., Qiu, S., Tian, J., Wen, X., Miller, J. L., von Deneen, K. M., Zhou, Z., Gold, M. S., & Liu, Y. (2013). Altered functional brain networks in Prader-Willi syndrome. *NMR in Biomedicine*, 26(6), 622–629.

Figures

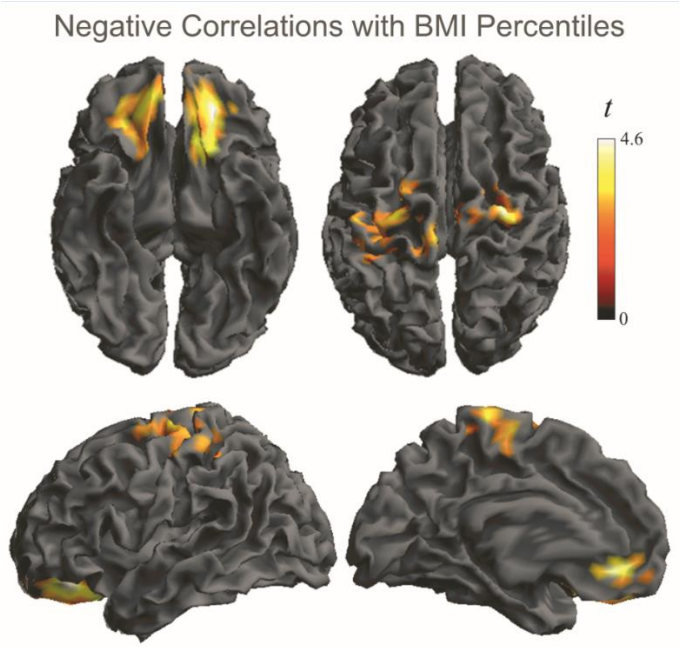

Figure 1. Brain areas showing a negative correlation between body mass index (BMI) percentiles and functional connectivity of the ventral striatum in the whole study sample.

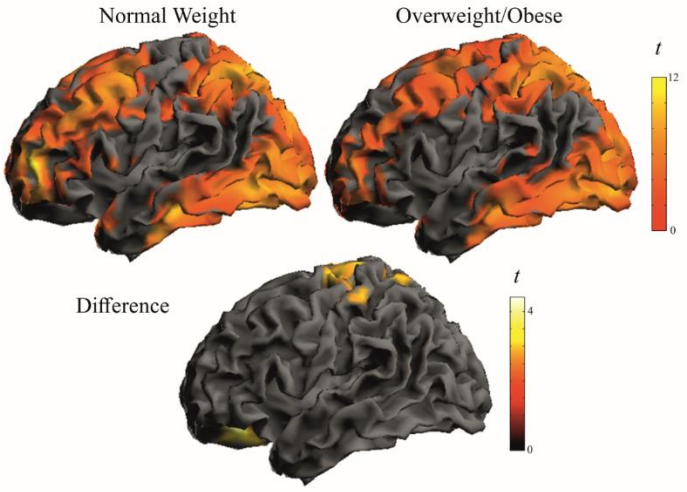

Figure 2. Brain areas anticorrelated (negative correlation) with the ventral striatum in normal weight and excess weight (overweight + obese) children (top), and significant differences between both groups (bottom) in the contrast normal > excess weight.

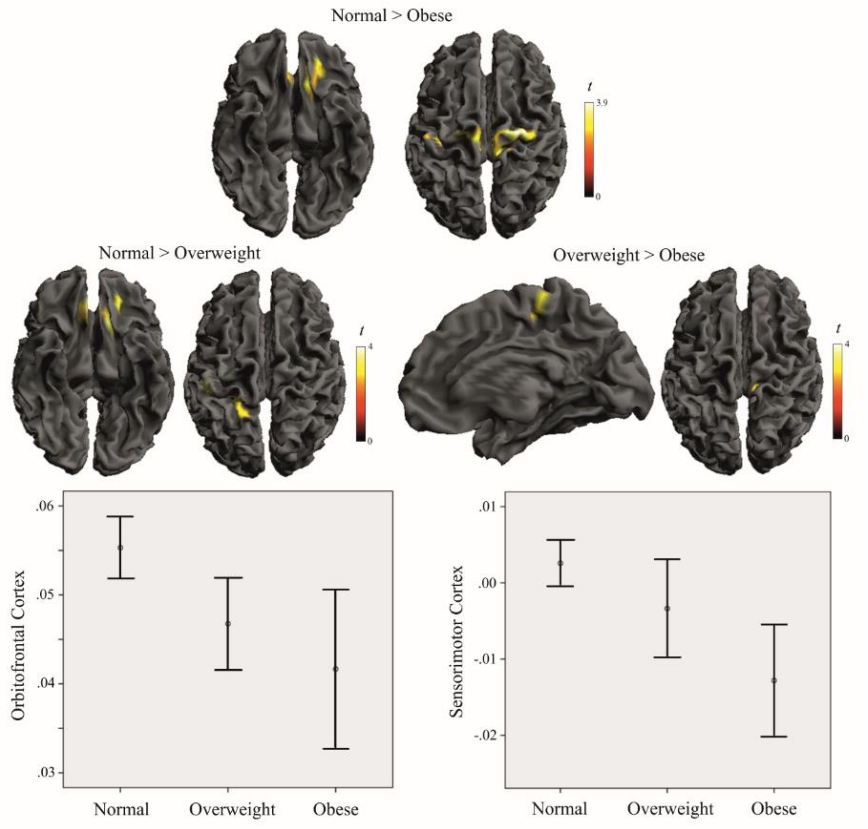

Figure 3. Differences in ventral striatum functional connectivity between WHO weight categories (top rows) and plots of individual data extracted at peak differences in the contrast normal weight > obese children. Vertical axis expresses mean group values and 95% CI of ventral striatum functional connectivity beta estimates.

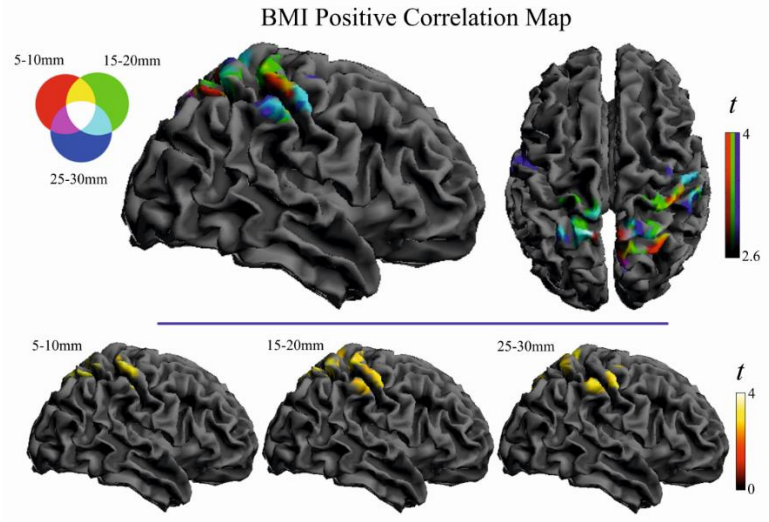

Figure 4. Correlations between BMI percentiles and cortical functional connectivity Iso-Distance Average Correlations (IDAC) measures in the whole study sample. All findings correspond to positive associations (i.e., higher BMI with stronger connectivity).

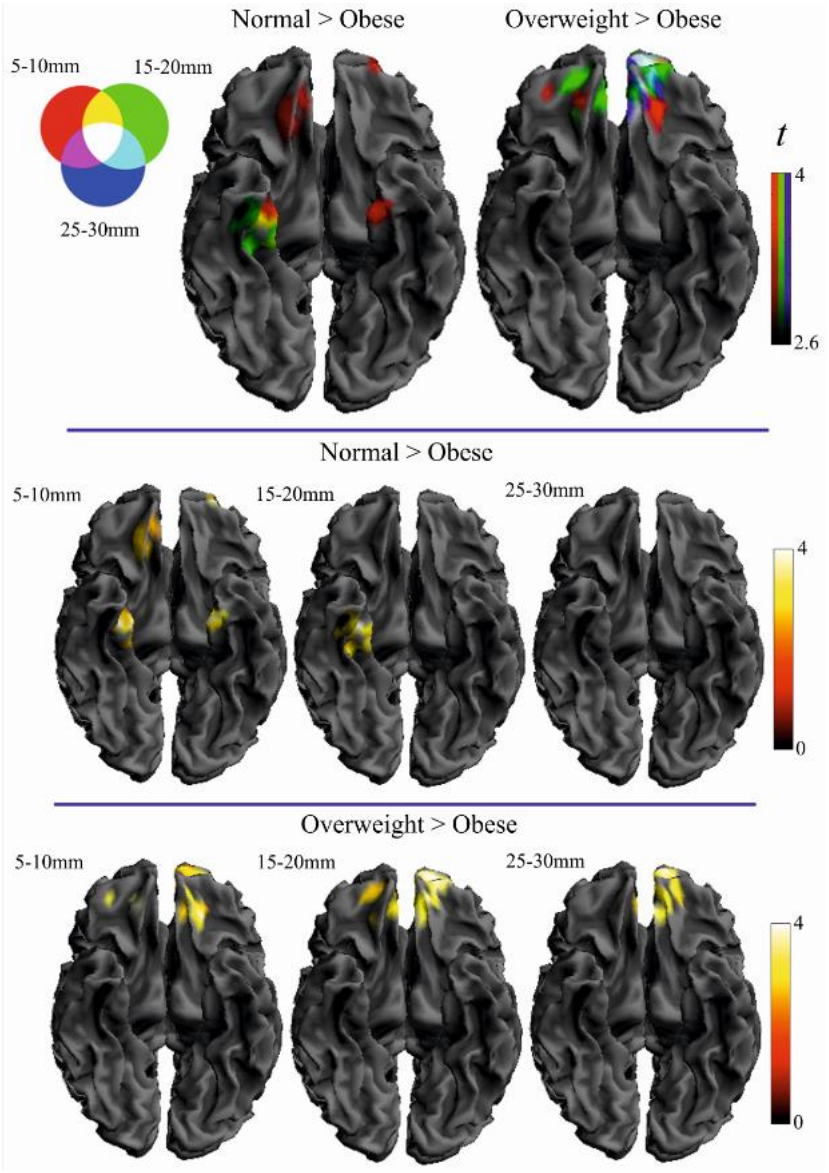

Figure 5. Differences in Iso-Distant Average Correlation (IDAC) measures between WHO weight categories.

Supporting Information

Dysfunctional brain reward system in child obesity

Supplementary Tables

Suppl. Table 1. Correlations between BMI percentile and functional connectivity of the ventral striatum in the whole study sample.

	Cluster size, ml	$P_{FWE\text{-}corr}$	*Peak x y z*	*T*	*P*
L Sensorimotor Cortex	23.0	0.00001	-26 -18 66	3.6	0.0002
R Sensorimotor Cortex	"	"	30 -16 68	4.7	3e-6
Medial Sensorimotor Cortex	"	"	0 -18 64	3.6	0.0002
L Orbitofrontal Cortex	15.6	7e-5	-22 38 -18	4.6	3e-6
R Orbitofrontal Cortex	12.7	0.0004	12 44 -6	4.6	4e-6

BMI, Body Mass Index. All findings correspond to negative associations (i.e., higher BMI with weaker connectivity). $P_{FWE\text{-}corr}$, P (Family-Wise Error corrected). x y z, coordinates given in Montreal Neurological Institute space.

Suppl. Table 2. Group differences in functional connectivity of the ventral striatum according to WHO weight status.

	Cluster size, ml	$P_{FWE\text{-}corr\ Cluster}$	*Peak x y z*	*T*	*P*
Normal > excess weight (overweight + obese)					
L Sensorimotor Cortex	17.4	0.00003	-24 -18 66	3.9	7e-5
R Sensorimotor Cortex	"	"	28 -16 68	4.7	2e-6
Medial Sensorimotor Cortex	"	"	-8 -26 70	3.7	0.0001
L Orbitofrontal Cortex	11.1	0.0009	-14 26 -20	4.3	1e-5
R Orbitofrontal Cortex	6.5	0.02	12 44 -6	4.3	1e-5
Normal > obese					
L Sensorimotor Cortex	15.1	0.00009	-34 -22 46	3.5	0.0003
R Sensorimotor Cortex	"	"	26 -16 70	4.0	4e-5
Medial Sensorimotor Cortex	"	"	-4 -26 66	3.7	0.0001
L Orbitofrontal Cortex	6.4	0.02	-32 42 -22	3.7	0.0001
R Orbitofrontal Cortex	1.9	*	12 44 -6	3.5	0.0003
Normal > overweight					
L Sensorimotor Cortex	4.4	*	-50 -30 56	3.5	0.0002
L Orbitofrontal Cortex	5.5	0.04	-12 24 -20	3.7	0.0001
R Orbitofrontal Cortex	"	"	6 32 -26	3.8	0.0001
Overweight > obese					
L Sensorimotor Cortex	1.6	*	8 -30 64	3.2	0.0009

$P_{FWE\text{-}corr}$, P (Family-Wise Error corrected). x y z, coordinates given in Montreal Neurological Institute space. *Subthreshold; significant with small volume correction within the region of interest.

Suppl. Table 3. Correlations between BMI percentile and cortical functional connectivity Iso-Distance Average Correlations (IDAC) measures in the whole study sample.

	IDAC distance	***Cluster size, ml***	$P_{FWE\text{-}corr}$	***Peak x y z***	***T***	***P***
L Somatosensory / Sup. Parietal	5-10mm	3.9	0.00004	-5 -78 57	4.6	3e-6
R Somatosensory / Sup. Parietal	5-10mm	15.0	9e-14	4 -60 72	4.7	3e-6
L Somatosensory / Sup. Parietal	15-20mm	10.6	5e-9	-8 -42 78	4.2	2e-5
R Somatosensory / Sup. Parietal	15-20mm	18.3	6e-13	31 -60 63	4.8	2e-6
L Somatosensory / Sup. Parietal	25-30mm	6.0	0.00003	-11 -48 75	4.6	4e-6
R Somatosensory / Sup. Parietal	25-30mm	15.9	3e-7	13 -63 72	4.8	1e-6

BMI, Body Mass Index. All findings correspond to positive associations (i.e., higher BMI with stronger connectivity). $P_{FWE\text{-}corr}$, P (Family-Wise Error corrected). x y z, coordinates given in Montreal Neurological Institute space.

Suppl. Table 4. WHO group differences as to cortical Iso-Distance Average Correlation (IDAC) measures: POSITIVE WEIGHT STATUS EFFECTS.

	IDAC distance	*Cluster size, ml*	$P_{FWE\text{-}corr\ Cluster}$	*Peak x y z*	*T*	*P*
Normal < excess weight (overweight + obese)						
R Somatosensory Cortex	15-20mm	3.4	0.001	46 -33 66	3.5	0.0003
R Superior Parietal	15-20mm	3.1	0.002	10 -72 63	4.1	3e-5
L Somatosensory Cortex	25-30mm	2.8	0.008	-50 -12 24	3.7	0.0001
R Somatosensory Cortex	25-30mm	2.1	0.04	49 -18 63	3.6	0.0002
Normal < obese						
		none				
Normal < overweight						
L Somatosensory Cortex	5-10mm	2.3	0.002	-2 -45 45	3.8	9e-5
R Superior Parietal	5-10mm	7.9	2e-8	4 -60 66	3.8	8e-5
R Somatosensory Cortex	5-10mm	1.5	0.04	46 -18 66	3.8	0.0001
R Superior Parietal	15-20mm	2.1	0.02	1 -54 45	4.1	3e-5
L Sensorimotor Cortex	25-30mm	2.2	0.02	-50 -12 24	3.4	0.0004
R Superior Parietal	25-30mm	4.7	0.0003	10 -78 60	3.9	5e-5
Overweight < obese						
		none				

$P_{FWE\text{-}corr}$, P (Family-Wise Error corrected). x y z, coordinates given in Montreal Neurological Institute space.

Supplementary Table 5. WHO group differences as to as to cortical Iso-Distance Average Correlation (IDAC) measures: NEGATIVE WEIGHT STATUS EFFECTS.

	IDAC distance	*Cluster size, ml*	$P_{FWE\text{-}corr\ Cluster}$	*Peak x y z*	*T*	*P*
Normal > excess weight (overweight + obese)						
R Amygdala Region	5-10mm	72	0.01	28 -12 -33	4.1	3e-5
Normal > obese						
L Orbitofrontal Cortex	5-10mm	2.9	0.0006	-14 72 0	3.9	7e-5
R Orbitofrontal Cortex	5-10mm	2.3	0.004	25 42 -21	3.5	0.0003
L Amygdala Region	5-10mm	1.9	0.01	-23 -12 -33	4.4	1e-5
R Amygdala Region	5-10mm	3.1	0.0004	31 -12 -33	4.3	1e-5
R Amygdala Region	15-20mm	5.4	3e-5	28 -12 -33	4.2	2e-5
Normal > overweight						
		none				
Overweight > obese						
L Orbitofrontal Cortex	5-10mm	6.4	6e-6	-20 -54 0	4.0	4e-5
R Orbitofrontal Cortex	5-10mm	1.9	0.01	19 39 -18	3.8	0.0004
L Orbitofrontal Cortex	15-20mm	9.1	6e-8	-11 48 -15	3.8	0.0001
R Orbitofrontal Cortex	15-20mm	2.9	0.004	1 42 -24	3.6	0.0002
L Orbitofrontal Cortex	25-30mm	6.8	8e-6	-8 60 -9	4.0	5e-5

$P_{FWE\text{-}corr}$, P (Family-Wise Error corrected). x y z, coordinates given in Montreal Neurological Institute space.

Supplementary Table 6. WHO group by distance interactions as to cortical Iso-Distance Average Correlation (IDAC) measures.

	Overall WHO Group-by-Distance Interactions				
	Cluster size, ml	$P_{FWE\text{-}corr}$	***Peak x y z***	**F**	***P***
R Orbitofrontal Cortex	3.5	1e-5	7 30 -18	7.3	9e-6
L Amygdala Region	5.2	6e-8	-23 -12 -30	10.5	3e-8
R Amygdala Region	5.1	1e-7	31 -12 -30	11.4	6e-9
	Post-Hoc Effects				
Short Distance Greater Effect *(Obese < Normal at short distance) > (Obese < Normal at long distance)*	***Cluster size, voxels***	$P_{FWE\text{-}corr}$	***Peak x y z***	***T***	***P***
L Orbitofrontal Cortex	1.9	0.02	-20 36 -21	4.3	1e-5
R Orbitofrontal Cortex	4.6	8e-5	19 36 -21	5.1	3e-7
L Amygdala Region	6.4	3e-6	-23 -9 -33	5.4	5e-8
R Amygdala Region	3.8	0.0004	22 -9 -30	5.0	4e-7

$P_{FWE\text{-}corr}$, P (Family-Wise Error corrected). x y z, coordinates given in Montreal Neurological Institute space.

Supplementary Figures

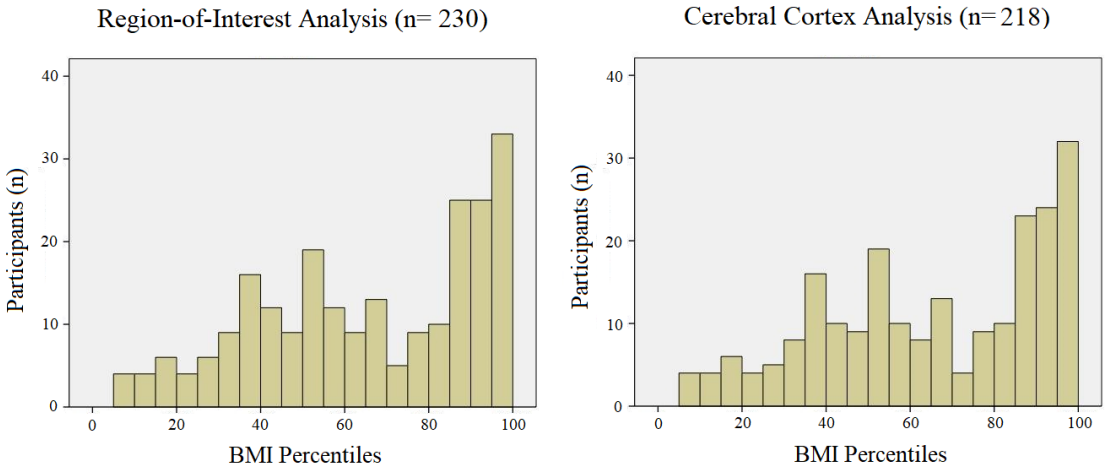

Supplementary Figure 1. Frequency histograms illustrating the distribution of body mass index (BMI) percentiles for participants included in both analyses.

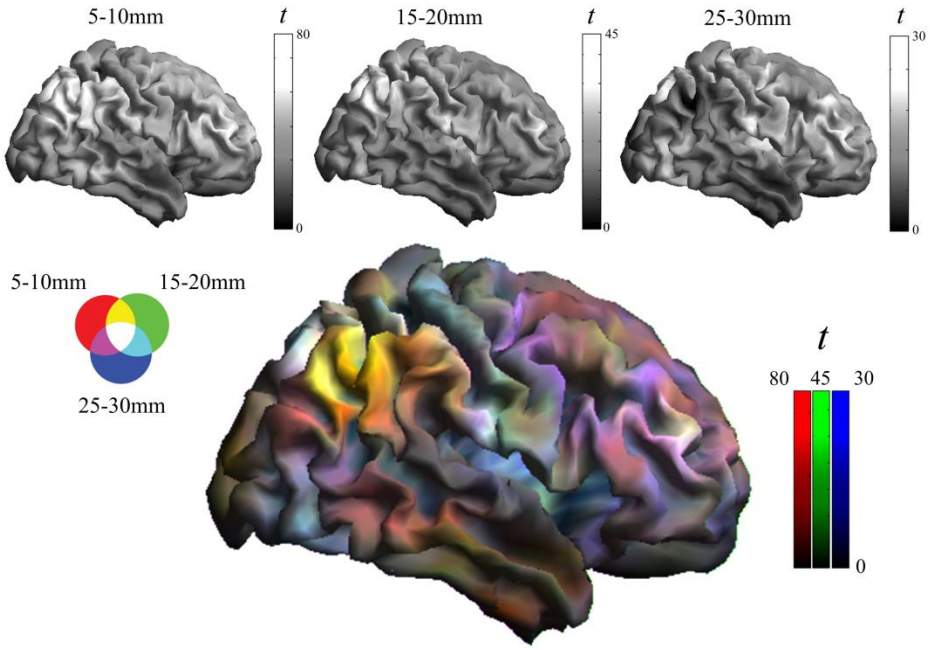

Supplementary Figure 2. One-sample Iso-Distant Average Correlation (IDAC) brain maps (normal-weight group). The gray images correspond to individual distance IDAC maps. The color image shows the result of superimposing the three IDAC maps using RGB (red, green and blue). The composite image is thus made up of primary RGB colors and their secondary combinations.

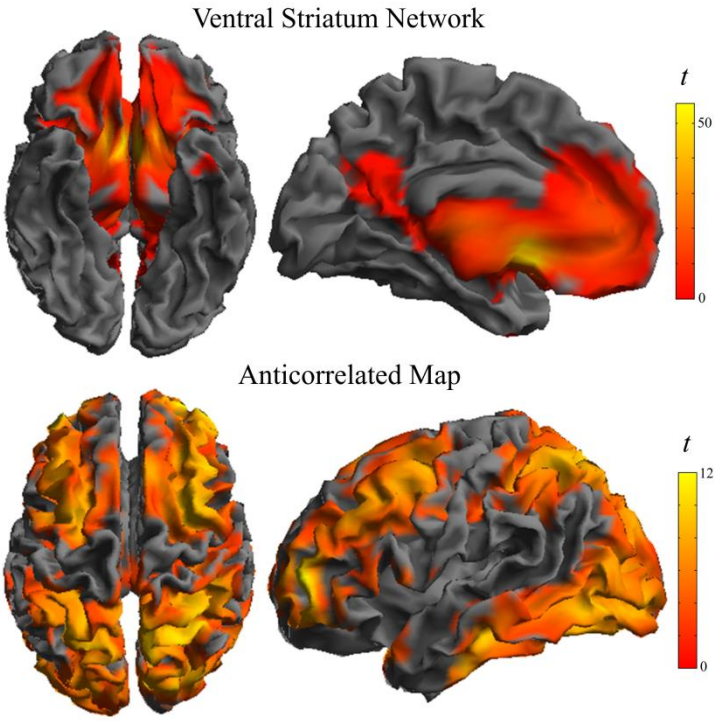

Supplementary Figure 3. One-sample maps for normal-weight children. The ventral striatum network corresponds to whole-brain positive correlations of the bilateral nucleus accumbens. The anticorrelation map corresponds to the nucleus accumbens' negative correlations.

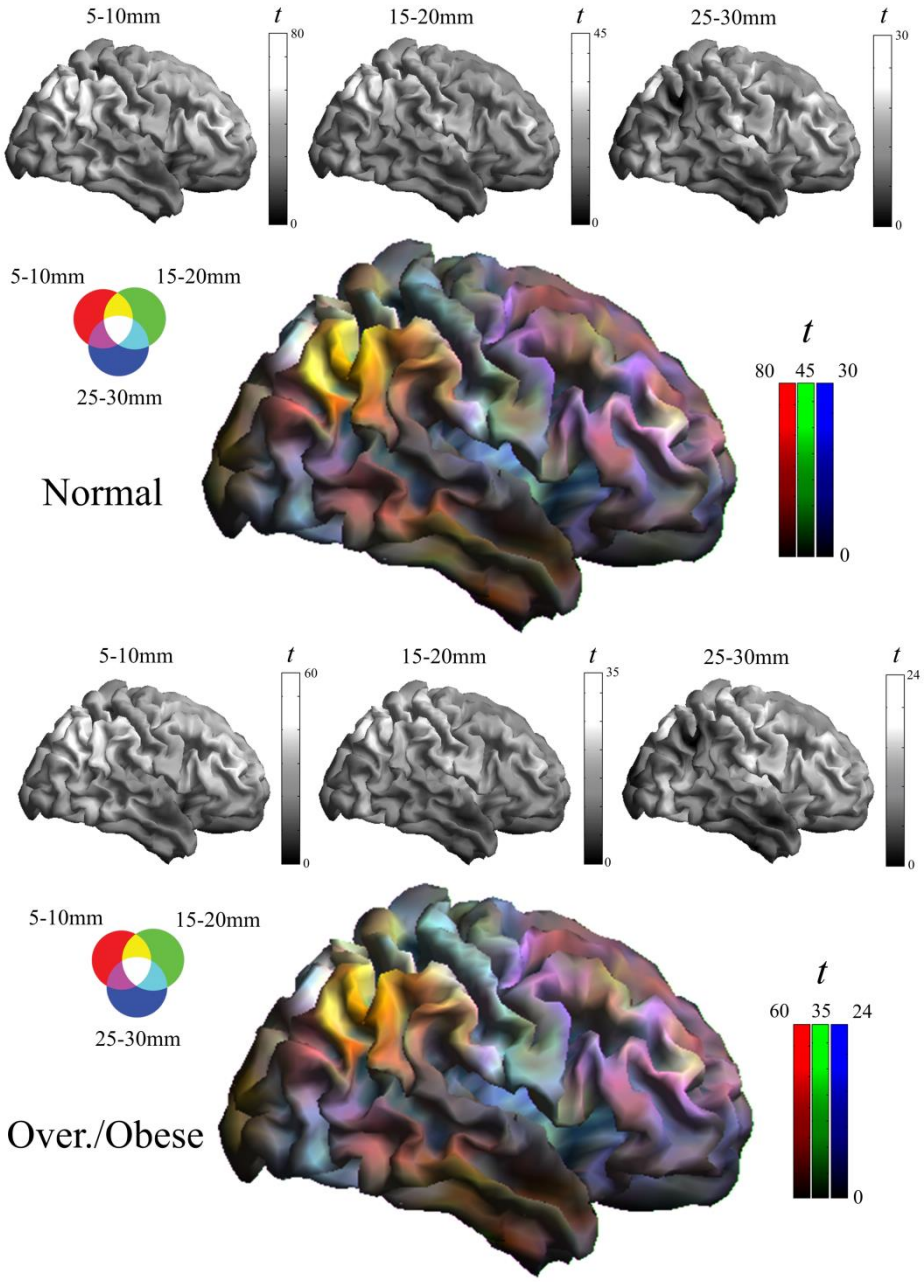

Supplementary Figure 4. One-sample Iso-Distant Average Correlation (IDAC) brain maps. The gray images correspond to individual distance IDAC maps. The color images show the result of superimposing the three IDAC maps using RGB (red, green and blue). The composite images are thus made up of primary RGB colors and their secondary combinations. Note that the differences between normal-weight (top) and excess-weight (bottom) children in the somatosensory cortex may already be appreciated upon visual inspection.

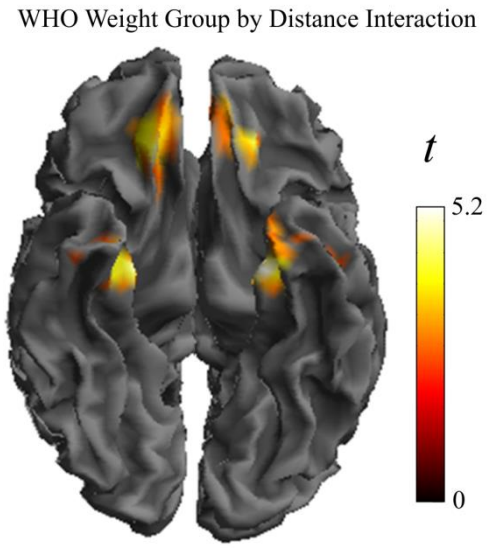

Supplementary Figure 5. Group (normal weight *vs* obese) by distance (5-10mm *vs* 25-30mm) interaction. The map shows areas with larger functional connectivity reduction in the obese group (compared with normal-weight children) at short than long local distance.

Supplementary Materials and Methods

Definition of Iso-Distant Average Correlation (IDAC)

We defined the concept of "Iso-Distant Average Correlation" (IDAC) to describe the pattern of correlation decay in the close vicinity of a voxel. $IDAC_i(h)$ was consequently defined as the average temporal correlation of voxel *i* with all the voxels located at a given Euclidean distance interval *h*. Functional MRI data sets being a discrete sample, any distance interval h must be necessarily transformed into a discrete iso-distant interval $H_k=(h_k, h_{k+1})$, with h_k being a set of successively increasing distances covering the whole vicinity of a given voxel(see Figure).

The set of iso-distant intervals H_k were selected so that temporal correlations were mainly positive, decreased monotonically and in which horizontal axon collaterals were considered likely to form local networks. For the present study, we defined 3 iso-distant intervals: 5-10mm, 15-20mm and 25-30mm, with constant thicknesses but increasing number of voxels.

We first computed a correlation matrix *C* of Pearson coefficients comparing the functional MRI signal time course of all the voxels in our study mask with each other's.

$$C_{i,j} = \frac{\sum_{k=1}^{M}\left(Y_{i,k} - \overline{Y_i}\right) \cdot \left(Y_{j,k} - \overline{Y_j}\right)}{\sqrt{\sum_{k=1}^{M}\left(Y_{i,k} - \overline{Y_i}\right)^2} \cdot \sqrt{\sum_{k=1}^{M}\left(Y_{j,k} - \overline{Y_j}\right)^2}}$$

where M is the length of the functional MRI signal time series and *i* and *j* index all the voxels entering our study mask. We then transformed the Pearson correlation matrix *C* into a Gaussian distributed z-score correlation matrix Z by applying a Fisher transform.

$$Z_{i,j} = \frac{\sqrt{M-3}}{2} \cdot \ln\left(\frac{1 + C_{i,j}}{1 - C_{i,j}}\right)$$

We obtained then $IDAC_i(h_k)$ by averaging the correlation coefficients of voxel *i* with all the voxels *j* belonging to the interval H_k.

$$IDAC_i(h_k) = \frac{\sum_{j \epsilon H_{k,i}} Z_{i,j}}{N_{k,i}}$$

In short, IDAC values are defined as the mean correlation z-score between one voxel's functional MRI signal and the functional MRI signal of all the voxels within the iso-distant interval $H_{k,i}$. Note that, for a given distance interval *k*, the number of voxels within the concentric iso-distant interval $N_{k,i}$ is not necessarily the same for every voxel *i* due to the edge effects of the study mask.

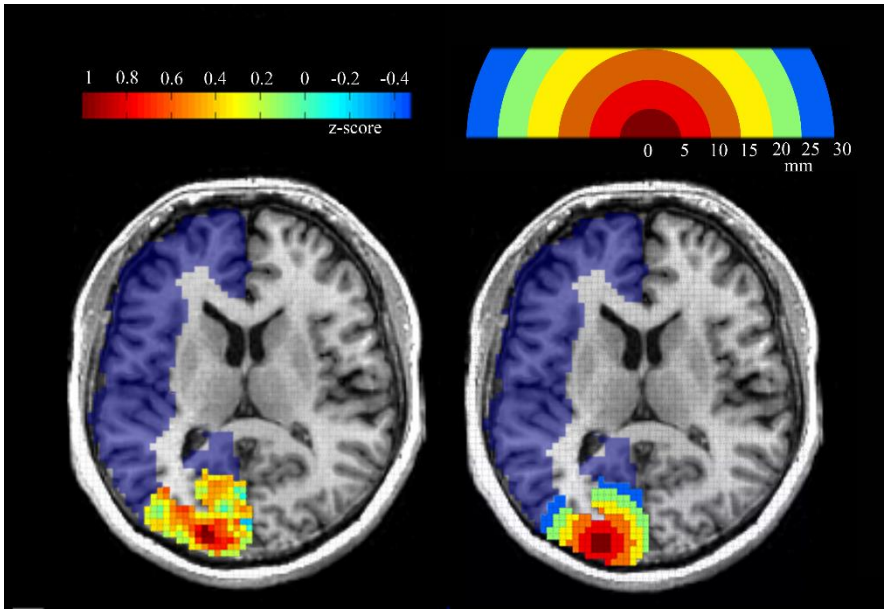

Figure. fMRI Temporal correlations between one voxel ("seed") and its neighboring peripheries present a characteristic decreasing spatial gradient. LEFT: Fisher-transformed z-scores of a correlation map with a "seed" voxel in the visual area from a single subject. Voxel resolution is 3x3x3mm and results are constrained to distance lags h_k<30mm and within the subject's native gray-matter mask (blue shade). RIGHT: Different Iso-distant intervals as they may be used to calculate different IDAC values.